ORIGINAL PAPER

Fabrication of a simple 3D-printed microfluidic device with embedded electrochemiluminescence detection for rapid determination of sibutramine in dietary supplements

Nisachon Praoboon[1] · Tanin Tangkuaram[1] · Viruntachar Kruefu[2] · Pusit Pookmanee[1] · Sirirat Phaisansuthichol[1] · Surasak Kuimalee[3] · Nattapol Laorodphan[3] · Sakchai Satienperakul[1]

Abstract

The design and fabrication of a simple 3D-printed platform with embedded electrochemiluminescence (ECL) detection for sibutramine determination is described. The microfluidic platform was fabricated by the fused deposition 3D-printing technique with polylactic acid filament, facilitated by computer-aided design (CAD). A three-electrode system was integrated into the device using graphene carbon paste as a working electrode, Ag/AgCl wire as a reference, and a graphite rod as a counter electrode. A further modification was carried out by applying bimetallic Au-Pt nanoparticle-supported multi-walled carbon nanotubes (MWCNT-Au-Pt) on the working electrode surface to enhance the electrocatalytic performance by exploiting the unique properties of nanomaterials. The analytical feasibility of the CAD-ECL sensor was tested through its application for the determination of sibutramine in dietary supplements. Under the optimized conditions, based on the enhancing effect of luminol emission, the device exhibited a linear calibration curve of the logarithmic sibutramine concentration versus ECL intensity in the range 5×10^{-3} to 1 ng mL^{-1}. The limit of detection was 3 pg mL^{-1} with a relative standard deviation of 1.7% ($n = 15$). The 3D-printed prototype can be successfully applied to a small-scale analysis in a simple and cost-effective approach.

Keywords Embedded electrochemiluminescence · 3D-printing technology · Sibutramine · Dietary supplements

Introduction

Microfluidic technology has become one of the well-established research platforms in numerous fields, including pharmaceutical analysis, clinical diagnosis, forensic science, food analysis, and environmental monitoring. Microfluidic platforms have advantages such as a miniaturized size, high portability, high-speed analysis, low production cost, low consumption of samples and reagents, and minimal waste generation [1]. Up-to-date microfluidic fabrication utilizes various substrates, such as metals, glass, and cellulose-based materials including paper or cloth due to the low cost and large availability of these raw materials [2]. Since the production of metal- or glass-based microfluidics platforms with a flexible design has been widely reported, the manufacturing process can be automated with high reproducibility and a wide choice of materials. However, the major drawbacks of metal and glass microfluidic chips are their high production costs and the requirement for advanced industry facilities and technical operators. Furthermore, the limitations related to the use of cellulose-based microfluidic devices include low mechanical resistance and the requirement of hydrophobic barriers to control and avoid the leakage of solutions. The drawbacks of those raw materials make thermoplastic and thermoset polymers the most useful options for use as low-cost microfluidic platforms [3].

In the early 2000s, microfluidic technologies based on micromolding in polymer substrates like polydimethylsiloxane (PDMS) received significant attention. Many microfluidic studies have been conducted by rapidly fabricating PDMS microfluidic devices to reduce costs and production time.

✉ Sakchai Satienperakul
sakchais@mju.ac.th

1. Department of Chemistry, Faculty of Science, Maejo University, Chiang Mai 50290, Thailand

2. Department of Physics, Faculty of Science, Maejo University, Chiang Mai 50290, Thailand

3. Department of Industrial Chemistry Innovation, Faculty of Science, Maejo University, Chiang Mai 50290, Thailand

Thermoplastic polymers, such as polystyrene, polyether ether ketone, polyethylene terephthalate, polyvinyl chloride, polymethylmethacrylate, and polycarbonate, have been commonly used in the fabrication of microfluidic chips. The option of fabrication using polymer materials was evaluated along with other elements. Various technologies, such as wet etching, conventional machining or reactive ion etching, soft lithography, photolithography, laser ablation, hot embossing, injection molding, in situ construction, and plasma etching, are available for fabricating polymeric microfluidic devices. Unfortunately, the manufacturing of polymer-based microfluidic chips still suffers from a relatively high production cost, and their mass production is time-consuming [4].

As a consequence, the current research strategy is focused on developing rapid fabrication methods without affecting the channel properties of the device. 3D-printing technology shows potential for this purpose because commercial 3D printers have been employed to easily create numerous analytical tools in recent years. 3D printers can construct items and complex models through one-step manufacturing, which allows for the integration of analytical chemistry devices and can be used on a small scale or in an isolated laboratory [5]. Moreover, computer-aided design (CAD) can be employed for the fabrication of new objects on demand [6]. 3D printing is a cost-effective microfabrication technique able to design and comfortably reproduce 3D objects at a low cost for diverse applications [7].

Among the detection techniques utilized in microfluidic devices, electrochemiluminescence (ECL) methods exhibit several advantages. The ECL mechanisms depend on the light-emitting compound, and the species that are associated with it. The ability to regenerate the reactive species in situ without an external light source for excitation allows for selective ultra-trace analyses [8]. Moreover, a simple instrumental setup, a high sensitivity, and a wide detection range can be applied to a small-scale platform with an easy and low-cost approach [9].

An electrochemical platform with a three-electrode configuration is commonly utilized in microfluidic chips [10]. The most common working electrode is based on graphite materials since carbon and carbon paste working electrodes demonstrate high performance. In addition, carbon materials can be enhanced by exploiting the unique properties of various nanomaterials, such as their small particle sizes and large surface areas that can accelerate electron transfer and reactions on the surface of the electrode [11]. Therefore, in the current study, bimetallic Au-Pt nanoparticle-supported multi-walled carbon nanotubes (MWCNT-Au-Pt) were used to enhance the ECL intensity during reactions.

As a proof of concept, the quantification of sibutramine (SIB) in dietary supplements was conducted using ECL sensing. Many earlier efforts have been described for SIB analysis using various instrumental techniques including high-performance liquid chromatography-electrospray ionization-mass spectrometry (HPLC-EI-MS) [12], gas chromatography-mass spectrometry (GC–MS) [13], ion-exchange chromatography (IEC) with conductivity detector [14], and liquid chromatography-mass spectrometry (LC/MS) [15], which provide good results with high sensitivity, reproducibility, and acceptability. Unfortunately, for resource-poor environments in remote areas, the high-cost instrumentation, time consumption, and requirements for trained technical personnel are often major limitations.

Recently, Karamahito et al. [16] reported a paper-based device for the quantitative measurement of sibutramine in slimming products, using Dragendorff's reagent for visual inspection. The proposed sensor was portable, user-friendly, and instrument-free. A limit of detection of 0.22 mM was observed for sibutramine adulteration screening.

Therefore, this report proposes a miniaturized, simple, rapid, and sensitive CAD-ECL sensor to determine SIB in weight-loss products. Moreover, the electrochemical performance of the CAD-ECL sensor with an embedded three-electrode system was enhanced by drop-casting MWCNT-Au-Pt particles on the carbon paste working electrode surface, which helped to substantially enhance electrocatalytic activity and the transfer of electrons during the ECL reactions. This contribution further expands the number of sensitive and specific detection modes of microfabrication by 3D-printing technology in food and pharmaceutical applications.

Materials and methods

Reagents and solutions

All chemicals were of analytical reagent (AR) grade and were used as received. SIB hydrochloride standard solution in methanol (1.0 mg mL^{-1}) was purchased from Sigma-Aldrich (USA). Standard solutions of SIB (5×10^{-6} to 1×10^{-3} µg mL^{-1}) were prepared daily with appropriate dilutions of the SIB stock solution with methanol (Merck, Germany). The stock solution of SIB hydrochloride was kept in a sealed container in a refrigerator at 4 °C when not in use.

A 0.1 M carbonate/bicarbonate buffer solution was prepared daily by dissolving the appropriate amount of Na$_2$CO$_3$ ($\geq$ 99%) and NaHCO$_3$ ($\geq$ 99.5%) (Sigma-Aldrich, USA), and the pH was adjusted to 9.6, using a 1.0 M NaOH solution. Ultra-pure deionized water (18.2 MΩ, Milli-Q Advantage A10 Water Purification System, France) was used for all solutions. A stock solution of luminol (0.1 M) was prepared by dissolving the appropriate amount of luminol ($\geq$ 97%) (Sigma-Aldrich, USA) in the 0.1 M carbonate/bicarbonate buffer (pH 9.6). The luminol reagent solution (1.0×10^{-2} M) was prepared fresh daily with the appropriate dilution of the luminol stock solution in the carbonate/bicarbonate buffer solution.

Dietary supplements (capsules) which may contain SIB were purchased from online commercial sources in Thailand. Ten capsules were accurately weighed, ground, and mixed. After grinding the capsule contents into a fine powder using a porcelain mortar, 1.0 g of the sample was dissolved in 10.0 mL of distilled water and sonicated for 2 min. The sample solutions prepared from these stock solutions were filtered through a 0.45-µm Nylon membrane (Millipore Corp., USA), and the SIB content was determined from the corresponding regression equation after appropriate dilution.

Preparation of the multi-walled carbon nanotubes-bimetallic Au-Pt nanoparticles

The MWCNT-Au-Pt nanoparticles and hybrid nanostructures (MWCNT-Au and MWCNT-Pt) were prepared using the method previously reported by Varol and Anik [17] with slight modifications. The methodologies are explained in this section step by step. First, multi-wall carbon nanotubes (MWCNT, > 98% carbon basis, 6–13 nm OD × 2.5–20 µm in length) (Sigma-Aldrich, USA) were soaked in a mixture of H_2SO_4 (75% v/v) and HNO_3 (25% v/v) under sonication for 6 h. Afterward, the pre-treated MWCNTs were washed with ultra-pure deionized water several times by centrifugation at 3500 rpm for 10 min for removing the excess acidic supernatant. The remaining solid carbon was kept in an oven overnight at 60 °C.

Platinum nanoparticles (Pt NP) were synthesized using a citrate reduction method. A solution mixture containing 1 mL of 8 mM potassium hexachloroplatinate (IV) ($K_2PtCl_6\cdot6H_2O$, ≥ 99.99%) (Sigma-Aldrich, USA) and 2 mL of 40 mM trisodium citrate (99%, Fluka, USA) was combined with 18 mL of deionized water and stirred at 200 rpm for 30 min. Then, 200 µL of $NaBH_4$ (50 mM) (Fisher Scientific, USA) was added to the solution until it turned into a dark-brown color (Pt NP solution). Finally, The Pt NP solution was left to cool down at room temperature and kept refrigerated at 4 °C. Gold nanoparticles (Au NPs) were synthesized using a similar process. Briefly, 15 mL of a 0.06% w/v gold (III) chloride trihydrate solution ($HAuCl_4$ $3H_2O$, ≥ 99.9%) (Sigma-Aldrich, USA) was brought to a boil, and 500 µL of a 10 mM trisodium citrate solution and 4 mL of 10 mM $NaBH_4$ were added. The solution mixture was stirred at 200 rpm for 20 min, and the color changed to a vibrant red (Au NP solution). The Au NP suspension was left to cool down and stored in the refrigerator at 4 °C.

Subsequently, the preparation of hybrid nanomaterials (MWCNT-Au, MWCNT-Pt, and MWCNT-Au-Pt) was performed based on a modified method from a previous study [18]. Binary nanohybrids of MWCNT-Au and MWCNT-Pt were prepared by sonicating mixed solutions with 10 mg of pre-treated MWCNT and 10 mL of Au NP or Pt NP suspensions for 4 h. The tertiary nanohybrid of MWCNT-Au-Pt was similarly prepared by mixing 10 mg of pre-treated MWCNTs and 5 mL of each Au NP and Pt NP suspension and then sonicated for 4 h. After sonication, all nanohybrids were dried at 60 °C overnight.

Design and fabrication of the 3D-printed CAD device

The 3D modeling of the CAD platform with an embedded three-electrode system was performed using Tinkercad, a free online 3D modeling program (Autodesk, San Rafael, CA, USA). A FlashForge 3D Printer (Zhejiang Flashforge 3D Technology Co., Ltd., China) equipped with a 0.4-mm diameter brass extruder nozzle was utilized with a temperature and printing speed of 200 °C and 20 mm s^{-1}, respectively. The general design of the six sets of CAD-ECL devices is illustrated in Fig. 1A. The 3D-printed platform was designed based on the conventional electrochemical cell with an embedded three-electrode system. Each basement of the CAD had dimensions of 8.80 mm length, 8.80 mm width, and 4.30 mm height with a 35 µL internal chamber volume that contained three holes for the embedded microelectrodes. The 3D model was downloaded as a stereolithography (.stl) file (Fig. 1A) and then uploaded to the slicer software using Flash Print. The prepared 3D model file was stored as a Geometry Expressions Document (.gx) file.
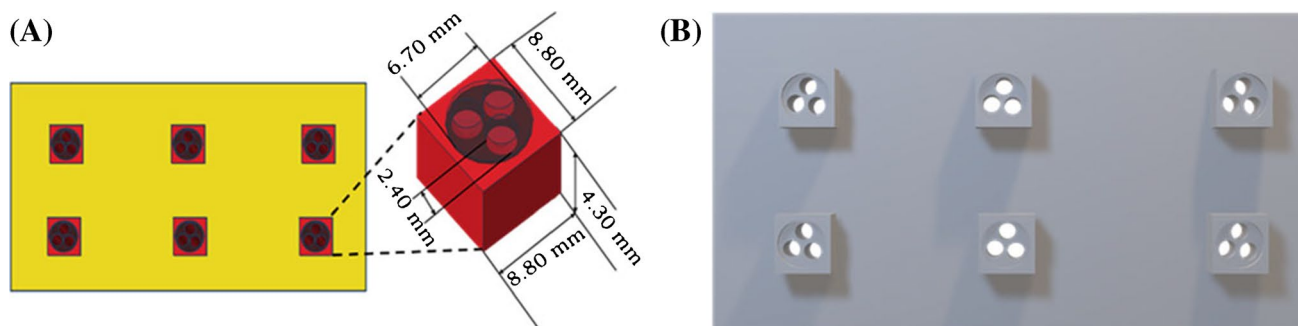
Fig. 1 **A** Digital model of the set of six devices designed through Tinkercad. **B** The 3D model was uploaded as a stereolithography file (.stl)

Afterward, the prepared object file was loaded onto an SD card and converted into a stereolithography format, and then, the printers executed each operation. Printing was carried out with a nonconductive filament of polylactic acid (PLA) (Zortrax, China).

CAD-ECL sensor fabrication

The ECL measurements for SIB detection were carried out through the embedded electrodes inside a 3D-printed electrochemical cell. The embedded CAD-ECL electrodes consisted of a carbon paste (CP) working electrode (WE) prepared from a packed homogeneous mixture of graphene powder and mineral oil, at an 80:20 (%wt.) ratio. An Ag/AgCl reference electrode (RE) was employed by inserting a 2-cm Ag wire into one hole, and subsequently, chlorination of the Ag wire surface was achieved by applying 5 µL of $FeCl_3$ (0.1 M) for 1 min and washing with water. A graphite rod was used as the counter electrode (CE). The electrical contacts from the rear side of the CAD-ECL device were established using stainless copper wires for connection to the CP-packed WE and restrained with epoxy resin (Fig. 2).

The CP-packed WE was modified by drop-casting 0.5 µL of MWCNT-Au-Pt nanomaterial suspension (1 mg mL^{-1} in 0.5% of chitosan) on the CP-packed WE. The modified CAD-ECL sensor was subsequently dried and kept in a desiccator prior to use.

Electrochemical studies using the CAD-ECL sensor

Cyclic voltammetry (CV) and electrochemical impedance spectroscopy (EIS) were employed to investigate the electrochemical behavior of the modified CP-packed WEs. A model electroactive species of 10 mM potassium ferricyanide in a potassium chloride solution (0.1 M) was used for studying the electrochemical characteristics. The conventional three-electrode system was set up in the CAD-ECL sensor, using different individual CP-packed WEs (including unmodified, chitosan (CHIT)-modified, MWCNT, MWCNT-Au, MWCNT-Pt, and MWCNT-Au-Pt-modified electrodes), a Pt wire as CE, and an Ag/AgCl RE (Metrohm, Switzerland). CV experiments were carried out in a potential range of −0.3 to 1.0 V, using a potentiostat (Autolab PGSTA101, Switzerland). EIS was also recorded using different modified WEs with the same electrolyte solution as the aforementioned.

ECL behavior of luminol on the CAD-ECL sensor

For the ECL measurement, the electrochemical reaction was initiated by the CV technique using a potentiostat. Prior to each ECL measurement, 30 µL of a 0.1 M luminol solution (dissolved in 0.1 M carbonate-bicarbonate buffer, pH 9.6) and 5 µL of a SIB standard or sample were introduced into the electrochemical cell, separately. The chemiluminescence light emission was triggered by CV at the sweeping potential of the CP-packed WE in the CAD device in a range of −0.5
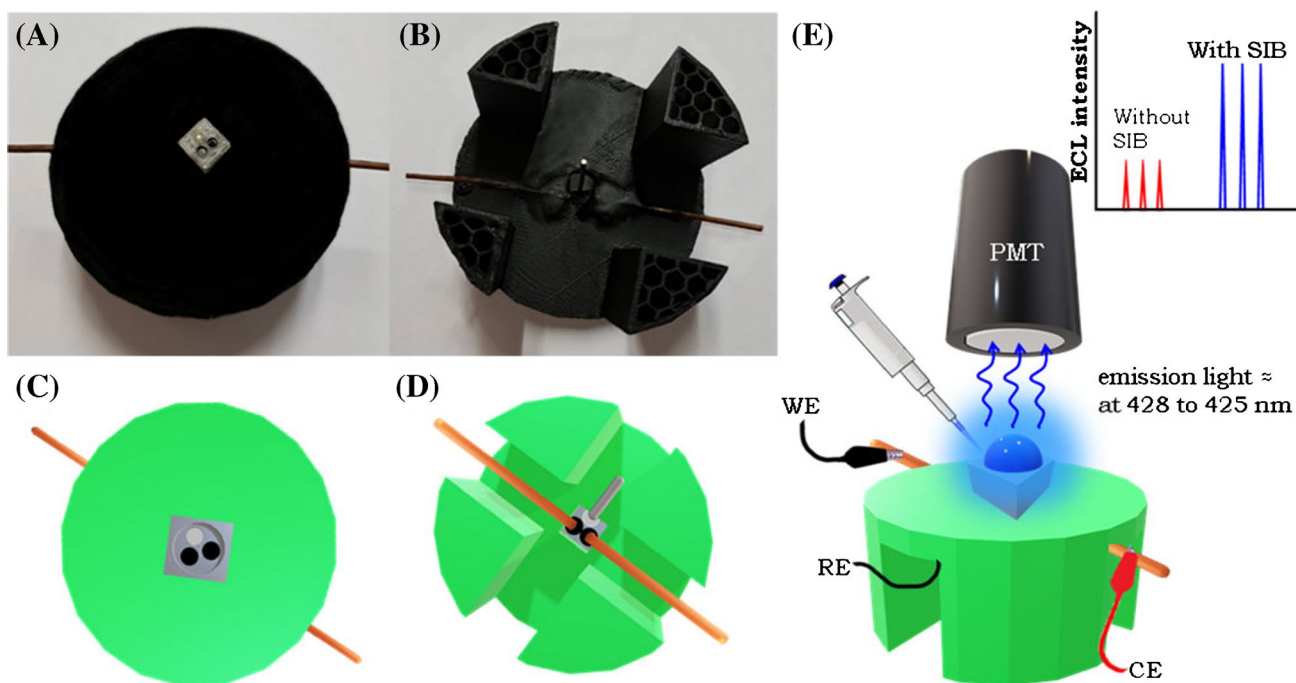
Fig. 2 An assembly of the 3D-printed ECL device for ECL detection: **A** top view and **B** bottom view; **C–D** CAD design of the base of the embedded CAD-ECL device with electrical connections; and **E** experimental setup for ECL measurements

to 1.0 V, with a scan rate of 75 mV s^{-1}. When the chemiluminescence light appeared in the CAD chamber, it was captured using a photomultiplier tube (PMT) (Thorn-EMI 9828SB, Electron Tubes Ltd., UK) and put in the sealed black box where the set of the CAD-ECL device was aligned directly in front of the PMT window. The applied potential for the PMT was set at 950 V, using a stable high-voltage power supply (Thorn-EMI model PM 20, Electron Tubes Ltd., UK). An output ECL signal was observed continually and exported to a personal computer, using a USB/RS-232 digital multimeter (UT60F, Hong Kong) through a voltage divider (C37BFN2, Electron Tubes, UK). The UNI-T® UT60F AC/DC software was employed for measuring the peak maximum. The increase in the ECL signal in the presence of the SIB standard or sample solution led to the analytical quantitation of SIB, where $\Delta I = I_s - I_0$. I_0 is the intensity of the luminol solution in the absence of SIB (1.0×10^{-2} M luminol reagent solution in 0.1 M carbonate-bicarbonate buffer, pH 9.6), and I_s is the intensity in the presence of a SIB standard or sample.

Results and discussion

In this work, we introduced a disposable ECL platform fabricated with PLA filament, using a commercial 3D printer. The analytical applicability of this CAD-ECL sensor was examined by detecting SIB. The quantification of SIB is important because SIB is considered a potentially harmful drug able to trigger adverse cardiovascular and neuropsychiatric disorders. The Food and Drug Administration (USA) and European Medicines Agency banned SIB because of its cardiovascular risks [18–20].

Design and fabrication of the 3D-printed devices

The CAD-ECL devices were designed in Tinkercad, which is a user-friendly software that can be used for free on most Internet browsers. Furthermore, Tinkercard contains many ready-made models and basic shapes. Figure 3 shows the six sets of 3D-printed devices. Each set contains three holes (2 mm inner diameter) for embedding the three-electrode system. The electrochemical chamber has a 7.5 mm inner

diameter with a maximum volume of 35 μL. For ECL analysis, a standard or sample containing SIB was loaded into the electrochemical chamber. The electrical connections were affixed directly to the electrodes when the electrochemical studies were carried out. These studies were performed at ambient temperature using an Autolab PGSTAT128N potentiostat/galvanostat. Therefore, the simple CAD-ECL sensor proposed in this study allows beginners to design and easily fabricate devices from available commercial polymer filaments and develop inexpensive polymer-based sensors using an available 3D printer instead of complicated photogrammetry software.

In addition, this study proposed the development of the embedded ECL detection using MWCNT-Au-Pt by dropcasting nanosuspensions onto the CP-packed WE surface for the ECL detection of SIB in the presence of luminol in an alkaline Na_2CO_3–$NaHCO_3$ buffer solution [21].

Morphology of the MWCNT-Au-Pt nanoparticles

The surface morphologies of the pre-treated MWCNTs and MWCNT-Au-Pt nanoparticles were investigated by scanning electron microscopy (SEM; Tescan, Vega III, Czech Republic) with a magnification of ×20.0 kV. The SEM surface view and corresponding elemental mapping of MWCNT-Au-Pt are shown in Fig. 4; these images were captured with the scanning electron microscope using energy dispersive spectroscopy (EDS). SEM images of the raw MWCNT (Fig. 4A) revealed a lump of entangled nanotubes with 6.05 mm diameters and tubular structures. In Fig. 4B, the MWCNT-Au-Pt nanoparticles showed semi-cylindrical shapes, decorated with agglomerated Pt NPs and Au NPs. Furthermore, the Au NPs and Pt NPs were evenly distributed on the MWCNTs (Fig. 4C–F). Most of the carbon species were observed in the MWCNT regions (Fig. 4C). However, the O, Pt, and Au maps were taken on the distributed area alike (Fig. 4D–F), which show the carboxylic acids (-COOH) on the MWCNT after acid treatment and the Au-Pt NPs, respectively. The EDS elemental mapping of the SEM image revealed that the metal nanoparticles were successfully decorated on the surfaces of the MWCNTs.

Fig. 3 Photograph of the CAD-ECL device. **A** The printed set of six devices. **B** Comparison of the CAD-ECL device with a 10-baht coin
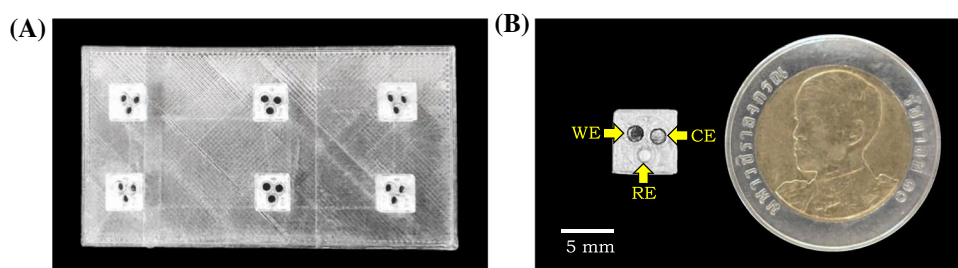
Fig. 4 Surface morphology of the MWCNT-Au-Pt nanoparticles. **A** Top-view SEM image of the pre-treated MWCNTs and **B** MWCNT-Au-Pt nanoparticles. EDS spectra and elemental mapping of the MWCNT-Au-Pt nanostructures composed of **C** carbon, **D** oxygen, **E** gold, and **F** platinum
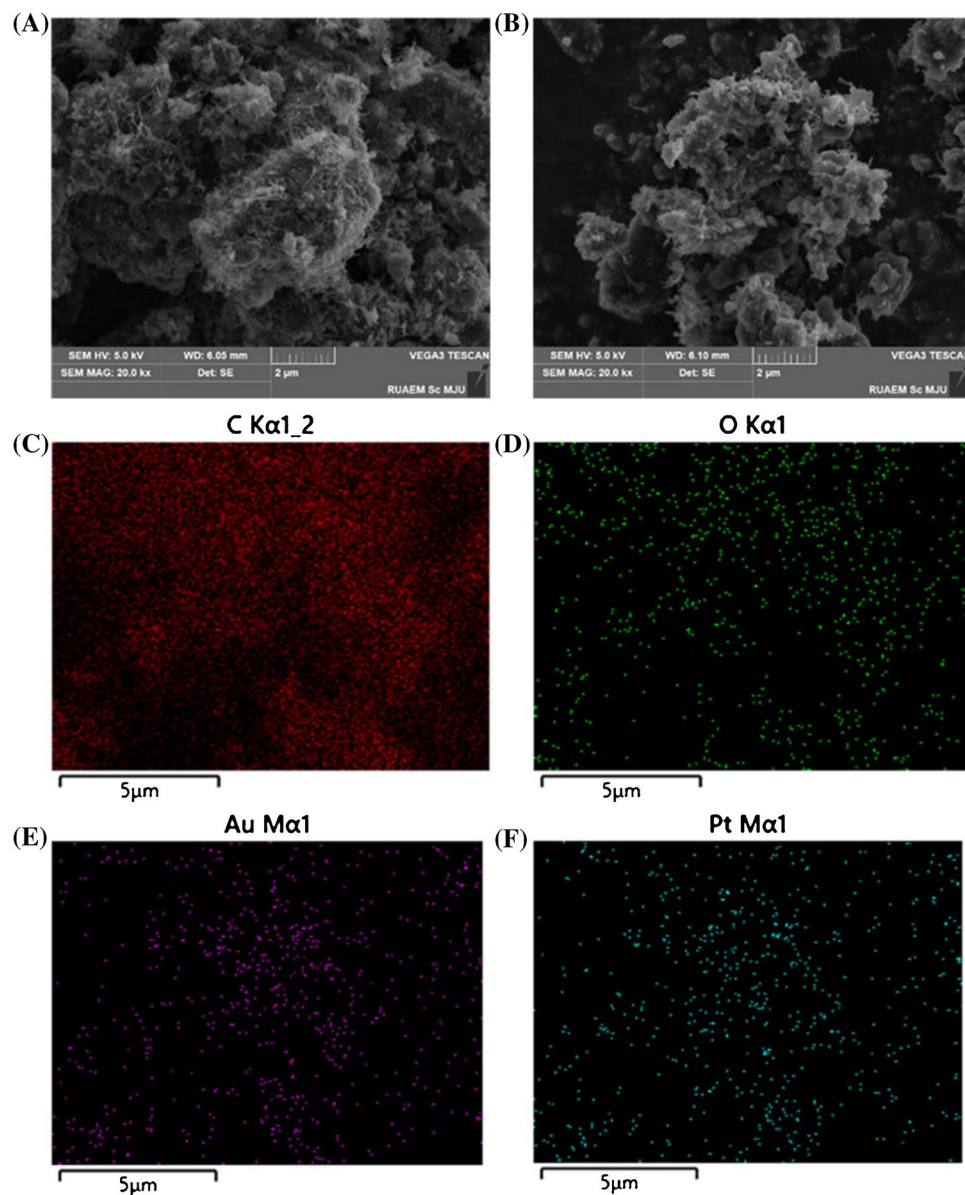
Electrochemical performance of the 3D-printed device

The electrocatalytic oxidation performance of the six CP-packed WEs (unmodified, CHIT-modified, CHIT-MWCNT, CHIT-MWCNT-Au, CHIT-MWCNT-Pt, and CHIT-MWCNT-Au-Pt-modified electrodes) was tested by CV, using 10 mM potassium ferricyanide in 0.1 M potassium chloride solution over a potential range from -0.3 to 1.0 V with a scan rate of 10 mV s^{-1}. The cyclic voltammograms of the stepwise individual modified electrodes are shown in Fig. 5A. Electron transfer occurred on each WE surface. The well-defined quasi-reversible redox peaks of $Fe(CN)_6^{3-}$ were recorded. In the case of the unmodified electrode (curve a), the redox peak currents were observed

at a lower current than that obtained from a CHIT-modified electrode (curve b), probably due to the chitosan-coated electrode having clusters of positive charge associated with the protonated amine groups of chitosan, which can interact with the negative charge of the $Fe(CN)_6^{3-}$ redox species [22]. Subsequently, the behavior of each modified electrode was investigated by observing changes in the redox peak currents. The MWCNT-modified electrode showed an increase in the redox peak current, which is the result of fast heterogeneous charge transfer and excellent electrochemical conductivity, owing to the edge plane sites in MWCNTs at the ends and along the tubes. The modified WEs using the Pt NPs, Au NPs, and MWCNT-Au-Pt showed a substantial and successive increase in the quasi-reversible redox peaks, which demonstrates the efficient electrocatalytic activity and
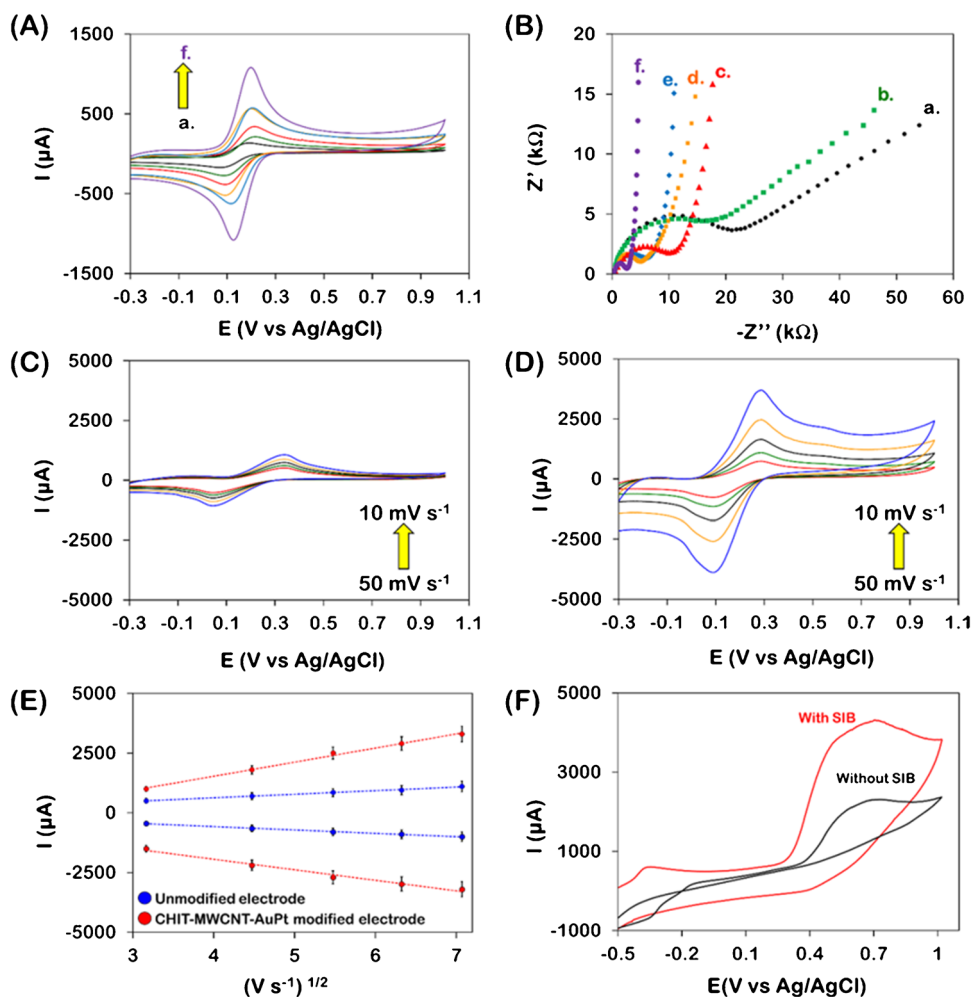
Fig. 5 The electrochemical studies were performed using 10 mM $Fe(CN)_6^{3-}$ in 0.1 M KCl on various CP-packed electrodes: unmodified (curve a), CHIT-modified (curve b), CHIT-MWCNT-modified electrode (curve c), CHIT-MWCNT-Au-modified electrode (curve d), CHIT-MWCNT-Pt-modified electrode (curve e), and CHIT-MWCNT-Au-Pt-modified electrode (curve f). **A** Cyclic voltammograms in a potential range from −0.3 to 1.0 V at a scan rate of 10 mV s^{-1}. **B**) Nyquist diagram of electrochemical impedance spectra recorded from 1 to 10,000 Hz. The electrode kinetic parameters on the CAD-ECL device using 10 mM $Fe(CN)_6^{3-}$ in 0.1 M KCl at scan rates from 10 to 50 mV s^{-1}. **C** Cyclic voltammograms of the unmodified electrode and **D** CHIT-MWCNT-Au-Pt-modified electrodes. **E** The comparison of the relation plot between the anodic and cathodic current responses and the square root of the scan rates between the unmodified and modified electrodes. **F** Cyclic voltammograms of luminol on the CAD-ECL devices in the presence (red line) and absence (black line) of SIB in a 0.1 M luminol solution

the enhanced conductivity by the metallic nanoparticles as well as their high surface-to-volume ratios [23].

EIS measurements were performed, and the results were presented using Nyquist plots in a frequency range of 0.1–10,000 Hz. The semicircle section observed in the EIS plots was correlated with the limited process of electron transfer. The electron transfer resistance (R_{et}) at the electrode surface was equal to the semicircle diameter. Figure 5B illustrates the semicircle diameter of the Nyquist plot of −Z' against Z'. This demonstrates the electron transfer kinetics of the redox reaction at each electrode [24]. The unmodified CP-packed WE exhibited the largest semicircle (curve a). The semicircle diameter of the CHIT-modified

electrode (curve b) slightly decreased, whereas the semicircle diameters of the combined nanoparticle-modified WEs dramatically decreased (curves c–f). This may be due to the excellent conductivity of nanoparticles, which promote electron charge transfer and have a larger effective surface area. Thus, the data obtained in the EIS experiments agree with the CV technique because both sets of results indicate that the MWCNT-Au-Pt-modified electrode represents the most effective electron-conducting material in this study.

Electrode kinetic parameters are affected by the potential difference established across a layer immediately adjacent to the electrode surface. Kinetic measurements of the CHIT-MWCNT-Au-Pt-modified electrode were studied and

compared with the unmodified electrode. The scan rates of the CV varied from 10 to 50 mV s^{-1}. The responses of the unmodified electrodes are shown in Fig. 5C, while the response of the CHIT-MWCNT-Au-Pt modified electrode increases considerably as seen in Fig. 5D. When the scan rates step up, both anodic (I_{pa}) and cathodic (I_{pc}) current peaks proportionally increase. The peak current (I_p) for a quasi-reversible process exhibits a linear reliance on the anodic and cathodic peak currents with respect to the square root of the scan rates voltammetric responses, illustrated in Fig. 5E.

The diffusion coefficient value (D) can be used to explain whether an analyte is freely diffusing in a solution [25]. Furthermore, the electroactive surface area (Ae) of the electrode is a key parameter for determining the number of reaction sites, which in turn controls the rate of the chemical reaction and energy generation [26]. They can be calculated using the Randles–Sevcik equation. The surface concentration of the modified electrode was calculated using the Brown–Anson model [27]. The approximated values of the electrode kinetic parameters of the diffusion coefficient value (cm s^{-1}), electroactive surface area (mm^2), and surface concentration (mol cm^{-2}) for the optimal modified electrode were 7.5×10^{-6} cm s^{-1}, 5.0 cm^2, and 2.08×10^{-3} mol cm^{-2}, respectively. For the unmodified CP electrode, the corresponding values were 3.45×10^{-6} cm s^{-1}, 4.50 cm^2, and 9.50×10^{-4} mol cm^{-2}, respectively.

The electrochemical effect of SIB on the luminol behavior on the CHIT-MWCNT-Au-Pt-modified electrode was studied using 0.1 M luminol in carbonate-bicarbonate buffer (pH 9.4). As shown in Fig. 5F, luminol exhibits a reasonable electrochemical response that was not accompanied by a cathodic current, indicating an irreversible oxidation process on the modified electrode [28]. The oxidation peak potential around $+0.65$ V vs. Ag/AgCl was enhanced twofold in the presence of 1 µg mL^{-1} SIB.

ECL behavior of the 3D-printed device

A preliminary investigation of the ECL characteristics of each modified WE on the CAD-ECL devices was performed to illustrate the feasibility of SIB quantification using the proposed CAD-ECL device. The ECL intensities of luminol in the absence and presence of SIB were investigated under conventional CV in an alkaline carbonate-bicarbonate buffer (pH 9.4). A potential was applied in the range of -0.5–1.0 V with a scan rate of 50 mV s^{-1}. As shown in Fig. 6, weak ECL intensities of luminol were observed for the unmodified electrode (curve a). Similar ECL intensities were observed for the CHIT-modified electrode (curve b). The ECL intensities steeply rose for the MWCNT-modified electrode (curve c), while the intensities of both the MWCNT-Au- and MWCNT-Pt-modified electrodes substantially increased (curves d and e). The ECL intensity increased by at least five-fold (curve f) for the MWCNT-Au-Pt-modified electrode, which is likely to be attributed to the high electrocatalytic effects of MWCNT-Au-Pt on the working electrode.

Furthermore, the MWCNT-Au-Pt-modified electrode was tested by increasing the concentration of the SIB standard solution to 1 and 5 µg mL^{-1} (curves g–h). These experimental results indicate that ECL is related synergistically to the intensities generated by MWCNT-Au-Pt, as suggested in previous studies [29], for application in SIB quantification.

The ECL detection mechanisms of luminol/sibutramine in alkaline solutions have been proposed by Wang et al. [21]. The possible ECL mechanisms of SIB detection in aqueous alkaline solutions are simplified and depicted in Fig. 7. The oxidation of

Fig. 6 Comparison of ECL intensities from 0.1 M luminol in carbonate-bicarbonate buffer (pH 9.4) in the absence and presence of SIB, achieved in the individually CP packed CPWEs: (a) bare electrode, (b) CHIT-modified electrode, (c) CHIT-MWCNT-modified electrode, (d) CHIT-MWCNT-Au-modified electrode, (e) CHIT-MWCNT-Pt-modified electrode, (f) CHIT-MWCNT-Au-Pt-modified electrode, (g) 1 µg mL^{-1} SIB, (h) 5 µg mL^{-1}. The inset shows a cyclic voltammogram comparison with similar conditions as those observed by ECL
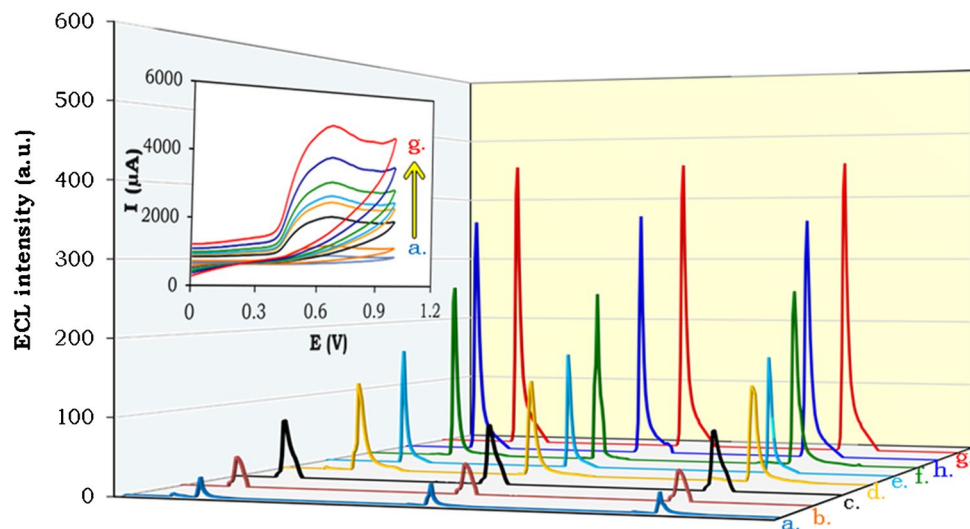
luminol at the electrode surface produces a diazaquinone intermediate ①. Meanwhile, SIB is oxidized and deprotonated and then reacted with the dissolved oxygen to form hydrogen peroxide species [30] ②. The hydrogen peroxide is then reacted with the diazaquinone intermediate to produce 3-aminophthalate in an excited state due to O–O bond cleavage in the endoperoxide form ③. The excited 3-aminophthalate then emits a characteristic blue light at 425 nm [31] ④. The emission intensity is proportional to the concentration of SIB in the solution media.

Analytical performance of the CAD-ECL device

To achieve the highest ECL intensity, the CHIT-MWCNT-Au-Pt-modified CAD-ECL sensor was used for the determination of SIB at a concentration of 0.5 μg mL^{-1}. The optimization of some parameters that affected the ECL

intensity was studied. The methodologies for determining the optimized conditions and parameters are described in the Electronic Supplementary Material.

Under the optimal conditions, the calibration plot is constructed, and the enhanced ECL intensity (ΔI) exhibits a linear relationship with the logarithmic SIB concentration (log c) for a series of standard concentrations between 5×10^{-3} and 1 ng mL^{-1}, as depicted in the inset of Fig. 8A. This result reveals a linear regression equation of $\Delta I = 497.3 \pm 0.1$ log c $+ 1114 \pm 1$, with a determination coefficient (R^2) of 0.995. The limit of detection, calculated based on three times of the standard deviation of the background signal, was determined to be 3 pg mL^{-1}. The LOD was calculated as three times the standard deviation of the response divided by the slope of the calibration curve at levels approximating the four lowest detectable concentrations [32].

Fig. 7 The possible mechanism of luminol/SIB detection on the CHIT-MWCNT-Au-Pt-modified CP-packed WE
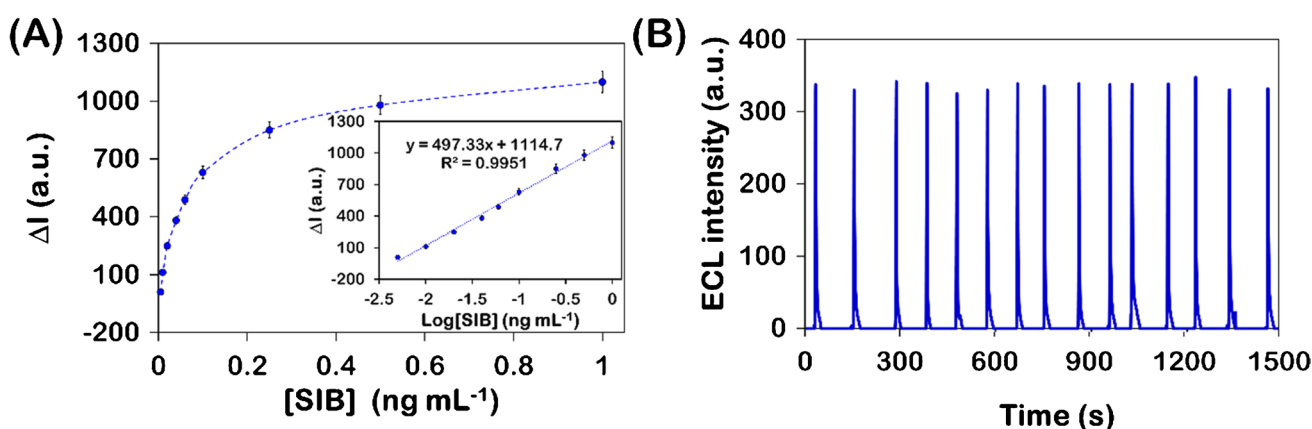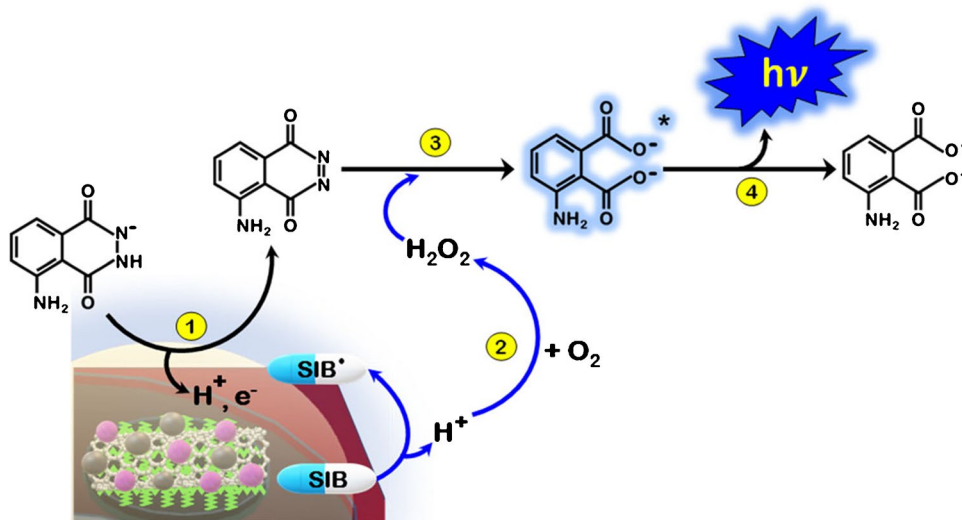
Fig. 8 A Calibration plot for the SIB determination using the CAD-ECL device under optimal conditions. The ECL responses were found to have a linear relationship with the logarithm SIB concentration over a concentration range between 5×10^{-3} and 1 ng mL^{-1} (inset). **B** The precision of the CAD-ECL device was attained by analyzing the SIB standard at a concentration of 2×10^{-2} ng mL.$^{-1}$

Table 1 Summary of the comparison of different methods for SIB detection in terms of linear range and detection limit

Method	Linear range (μg mL^{-1})	LOD (ng mL^{-1})	Reference
HPLC–ESI–MS	25–1000	15	[12]
GC–MS	1–500	17	[13]
Ion-exchange chromatography	10–500	2.3×10^6	[14]
Paper-based sensor	62–250	62×10^3	[16]
DPV	4×10^5–3.33×10^7	4×10^5	[30]
Smartphone-based colorimetry	1.4–4.2	360	[33]
FI-ECL	0.01–1.0	2.5	[21]
CAD-ECL	5×10^{-6}–1×10^{-3}	0.003	This work

Moreover, the reproducibility of the 3D-printed chips was investigated using 15 different printed microfluidic chips. The ECL intensity was examined by analyzing the SIB standard at a concentration of 2×10^{-2} ng mL^{-1} (Fig. 8B). The standard deviation (RSD%) of 15 measuremen

ts using the proposed CAD-ECL devices was calculated as 1.7%, indicating good repeatability and acceptability.

]Comparisons of this work with previous reports on SIB sensitivity are summarized in Table 1. The linear ranges and detection limits suggest that the proposed CAD-ECL sensor demonstrates more sensitivity than most of the well-known techniques. Moreover, the developed sensor is a cost-effective analytical platform. This sensor offers the advantages of simplicity and low-cost fabrication. Each CAD device was estimated to cost about 0.10 USD. Furthermore, PLA is biodegradable under commercial composting conditions and breaks down within 12 weeks, making our proposed sensor more environmentally friendly because of the low use of chemicals and toxic waste generation.

Moreover, the surface modification of a carbon plate working electrode with MWCNT-Au-Pt particles can overcome the electrical resistance of the paste. However, the drawback is a relatively weaker modified electrode compared with bare solid electrodes. This greatly limits the repeatability and mechanical stability of the modified working electrode. Unsurprisingly, the ECL measurement was performed effectively on CAD only once, and the microfluidic platforms could not be reused.

Analysis of SIB in dietary supplements

To evaluate the applicability and reliability of the CAD-ECL sensor in practical applications, SIB from three commercially available diet pill supplements was determined under optimal experimental conditions. The samples were prepared following the method of Wang et al. [21] with slight modifications. All three capsule sample solutions were investigated using the proposed CAD-ECL method. Recovery tests were performed to evaluate the accuracy of this method. The individual samples were spiked with SIB standard at concentrations between 2×10^{-5} and 6×10^{-5} μg mL^{-1}, and the results

Table 2 Summary of the SIB found in dietary supplement samples

Samples	Amount of SIB (μg kg^{-1})[a]			Recovery (%)
	Unspiked	Added	Found	
1	ND*	0.20	0.17 ± 0.01	85
		0.40	0.45 ± 0.05	113
		0.60	0.59 ± 0.05	98
2	0.13 ± 0.01[b]	0.20	0.34 ± 0.05	105
		0.40	0.47 ± 0.02	85
		0.60	0.80 ± 0.10	112
3	0.04 ± 0.01[b]	0.20	0.26 ± 0.04	110
		0.40	0.42 ± 0.05	95
		0.60	0.61 ± 0.09	95

*Not detected (< 3 pg mL^{-1})

[a]Three replicate measurements were performed for all samples. Data are reported as average $\pm$ standard deviation

[b]The sample solution was diluted 30 times using 0.1 M carbonate-bicarbonate buffer (pH 9.6)

of the spiked samples were determined and compared to the known values of the standard SIB solutions added. The results are summarized in Table 2. These data illustrate the successful determination of the illegal SIB added to the diet pill supplements, using our developed CAD-ECL device.

Conclusions

This work reported a simple, rapid, sensitive, and disposable 3D-printed sensor for the determination of SIB, using the electrogenerated chemiluminescence of luminol with the aid of bimetallic nanoparticles. The developed CAD-ECL platforms are relatively cost-effective, reproducible, and can be fabricated using simple 3D-printing technology. The 3D digital model was obtained using the open access and user-friendly Tinkercad software. This proposed platform does not require high computing power or sophisticated equipment for designing and fabricating 3D objects, which are basic requirements for small research laboratories with low budgets and resource-poor environments.

The proposed CAD device also demonstrated high electrochemical and photochemical performance. Owing to these considerations, the CAD-ECL platform was applied successfully for the quantitation of illegal SIB added to dietary supplements with high sensitivity and a very low limit of detection and without complicated sample preparation.

Data Availability Data of this reasearch is included in the manuscript and supplementary material, any other data can be provided upon request.

Declarations

Conflict of interest The authors declare no competing interests.

References

1. Scott SM, Ali Z (2021) Fabrication methods for microfluidic devices: an overview. Micromachines 12(3):319. https://doi.org/10.3390/mi12030319

2. Niculescu A-G, Chircov C, CătălinaBîrcă A, Grumezescu AM (2021) Fabrication and applications of microfluidic devices: a review. Int J Mol Sci 22(4):2011. https://doi.org/10.3390/ijms22042011

3. McDonald JC, Duffy DC, Anderson JR, Chiu DT, Wu H, Schueller OJA, Whitesides GM (2000) Fabrication of microfluidic systems in poly(dimethylsiloxane). Electrophoresis 21(1):27–40. https://doi.org/10.1002/(SICI)1522-2683(20000101)21:1%3c27::AID-ELPS27%3e3.0.CO;2-C

4. Sima F, Sugioka K, Vázquez RM, Osellame R, Kelemen L, Ormos P (2018) Three-dimensional femtosecond laser processing for lab-on-a-chip applications. Nanophotonics 7(3):613–634. https://doi.org/10.1515/nanoph-2017-0097

5. Renner M, Griesbeck A (2020) Think and print: 3D printing of chemical experiments. J Chem Educ 97(10):3683–3689. https://doi.org/10.1021/acs.jchemed.0c00416

6. Ambrosi A, Pumera M (2016) 3D-printing technologies for electrochemical applications. Chem Soc Rev 45:2740–2755. https://doi.org/10.1039/C5CS00714C

7. Ho CM, Ng SH, Li KH, Yoon YJ (2015) 3D printed microfluidics for biological applications. Lab Chip 15(18):3627–3637. https://doi.org/10.1039/C5LC00685F

8. Richter MM (2004) Electrochemiluminescence (ECL). Chem Rev 104(6):3003–3036. https://doi.org/10.1021/cr020373d

9. Dai W, Zhao Z, Ma Y, Ye J, Jin J (2020) Development of miniaturized electrochemiluminescence instrument using multi-pixel photon pounter as the optical detector. Electroanalysis 32:1–10. https://doi.org/10.1002/elan.202000094

10. Teymourian H, Moonla C, Tehrani F, Vargas E, Aghavali R, Barfidokht A, Tangkuaram T, Mercier PP, Dassau E, Wang J (2020) Microneedle-based detection of ketone bodies along with glucose and lactate: toward real-time continuous interstitial fluid monitoring of diabetic ketosis and ketoacidosis. Anal Chem 92(2):2291–2300. https://doi.org/10.1021/acs.analchem.9b05109

11. Sheng Q, Luo K, Zheng J, Zhang H (2008) Enzymatically induced formation of neodymium hexacyanoferrate nanoparticles on the glucose oxidase/chitosan modified glass carbon electrode for the detection of glucose. Biosens Bioelectron 24:429–434. https://doi.org/10.1016/j.bios.2008.04.024

12. Huang Z, Xiao S, Luo D, Chen B, Yao S (2008) Simultaneous determination of sibutramine and N-Di-desmethylsibutramine in dietary supplements for weight control by HPLC-ESI-MS. J Chromatogr Sci 46(8):707–711. https://doi.org/10.1093/chromsci/46.8.707

13. Khazan M, Hedayati M, Kobarfard F, Askari S, Azizi F (2014) Identification and determination of synthetic pharmaceuticals as adulterants in eight common herbal weight loss supplements. Iran Red Crescent Med J 16(3):e15344. https://doi.org/10.5812/ircmj.15344

14. Molin TRD, da Silveira GD, Leal GC, Müller LS, Carvalho Muratt DT, LM, de Ciana C, (2019) A new approach to ion exchange chromatography with conductivity detection for adulterants investigation in dietary supplements. Biomed Chromatogr 33(11):e4669. https://doi.org/10.1002/bmc.4669

15. Strano-Rossi S, Colamoici C, Botrè F (2007) Oxidized carbon nanotubes as matrix for matrix-assisted laser desorption/ionization time-of-flight mass spectrometric analysis of biomolecules. Rapid Commun Mass Spectrom 21(2):79–88. https://doi.org/10.1002/rcm.1779

16. Karamahito P, Sitanurak J, Nacapricha D, Wilairat P, Chaisiwamongkhol K, Phonchai A (2021) Paper device for distance-based visual quantification of sibutramine adulteration in slimming products. Microchem J 162:105784. https://doi.org/10.1016/j.microc.2020.105784

17. ÖrenVarol T, Anik Ü (2019) Fabrication of multi-walled carbon nanotube–metallic nanoparticle hybrid nanostructure based electrochemical platforms for sensitive and practical colchicine detection. New J Chem 43(34):13437–13446. https://doi.org/10.1039/C9NJ03227D

18. FDA Government (2022) FDA drug safety communication: FDA recommends against the continued use of meridia (Sibutramine), US Food and Drug Administration. http://www.fda.gov/drugs/drugsafety/ucm228746.htm. Accessed 30 Sept 2022

19. European Medicines Agency (2022) Questions and answers on the suspension of medicines containing sibutramine. http://www.ema.europa.eu/docs/en_GB/document_library/Referrals_document/Sibutramine_107/WC500094238.pdf. Accessed 30 Sept 2022

20. Ozdemir B, Sahin I, Kapucu H, Celbis O, Karakoc Y, Erdogan S, Onal Y (2012) How safe is the use of herbal weight-loss products sold over the Internet? Hum Exp Toxicol 32(1):101–106. https://doi.org/10.1177/0960327112436407

21. Wang S, Yu J, Wan F, Ge S, Yan M, Zhang M (2011) Determination of sibutramine with a new sensor based on luminol electrochemiluminescence. J Lumin 131(7):1515–1519. https://doi.org/10.1016/j.jlumin.2011.03.038

22. Chen H-J, Zhang Z-H, Lou L-J, Yao S-Z (2012) Surface-imprinted chitosan-coated magnetic nanoparticles modified multi-walled carbon nanotubes biosensor for detection of bovine serum albumin. Sens Actuators B Chem 163:76–83. https://doi.org/10.1016/j.snb.2012.01.010

23. Lin Z, Huang L, Liu Y, Lin J-M, Chi Y, Chen G (2008) Electrochemiluminescent biosensor based on multi-wall carbon nanotube/nano-Au modified electrode. Electrochem Commun 10:1708–1711. https://doi.org/10.1016/j.elecom.2008.08.028

24. Wu X, Zhong X, Chai Y, Yuan R (2014) Electrochemiluminescence acetylcholine biosensor based on biofunctional AMs-AChE-ChO biocomposite and electrodeposited graphene-Au-chitosan nanocomposite. Electrochim Acta 147:735–742. https://doi.org/10.1016/j.electacta.2014.10.016

25. Sandford C, Edwards MA, Klunder KJ, Hickey DP, Li M, Barman K, Sigman MS, White HS, Minteer SD (2019) A synthetic chemist's guide to electroanalytical tools for studying reaction mechanisms. Chem Sci 10(26):6404–6422

26. Zhu P, Zhao Y (2019) Cyclic voltammetry measurements of electroactive surface area of porous nickel: Peak current and peak charge methods and diffusion layer effect. Chem Phys 233:60–67. https://doi.org/10.1016/j.matchemphys.2019.05.034

27. Chauhan R, Singh J, Solanki PR, Manaka T, Iwamoto M, Basu T, Malhotra BD (2016) Label-free piezoelectric immunosensor decorated with gold nanoparticles: kinetic analysis and biosensing application. Sens Actuators B Chem 222:804–814. https://doi.org/10.1016/j.snb.2015.08.117

28. Uliana CV, Yamanaka H (2020) Simple, fast, and ultrasensitive method for textile dye determination based on luminol electrochemiluminescence (ECL) inhibition. J Solid State Electrochem 24:1927–1933. https://doi.org/10.1007/s10008-020-04571-9

29. Miao SS, Wu MS, Ma LY, He XJ, Yang H (2016) Electrochemiluminescence biosensor for determination of organophosphorous pesticides based on bimetallic Pt-Au/multi-walled carbon nanotubes modified electrode. Talanta 158:142–151. https://doi.org/10.1016/j.talanta.2016.05.030

30. Carvalho JM, de Silva AR, de Cunha ALMC, Aucélio RQ, Alberti ALM, Leandro KC (2012) Voltammetric determination of sibutramine in beverages and in pharmaceutical formulations. Quím Nova 35(5):988–992. https://doi.org/10.1590/S0100-40422012000500023

31. Marquette CA, Blum LJ (2008) Electro-chemiluminescent biosensing. Anal Bioanal Chem 390:155–168

32. Miller JC, Miller JN (2010) Statistics for analytical chemistry, 6th edn. Ashford Colour Press, Gosport

33. Chaisiwamongkhol K, Labaidae S, Pon-in S, Pinsrithong S, Bunchuay T, Phonchai A (2020) Smartphone-based colorimetric detection using gold nanoparticles of sibutramine in suspected food supplement products. Microchem J 158:105273. https://doi.org/10.1016/j.microc.2020.105273